

S-Shaped Current–Voltage Characteristics in Solar Cells: A Review

Rebecca Saive 

Abstract—S-shaped current–voltage (I – V) characteristics are a frequently occurring hurdle in the development of new solar cell material combinations and device architectures. Their presence points to the existence of a charge transport bottleneck that needs to be removed in order to unlock high fill factors and power conversion efficiencies. In this review, examples of studies in which s-shaped I – V curves have appeared are presented, and the cause and mitigation are discussed. Different solar cell material systems are often treated by separate communities, thereby, also the physics of s-shaped I – V curves have been treated separately. This review covers the main solar cell technologies—silicon, thin film, organic, hybrid—with the aim to provide an overarching picture of the common mechanisms and universal guidelines for mitigation of s-shaped I – V characteristics in emerging solar cell technologies. Except for a few studies on organic solar cells, s-shaped I – V curves are reported to result from charge transport barriers at one of the (selective) contact layers that can be overcome by interface engineering and doping.

Index Terms—Current–voltage characteristics, s-shape, roll over.

I. INTRODUCTION

WE HAVE entered an age in which solar cells are the most cost-efficient way to generate electricity in many regions of the world. This exciting development for all solar energy advocates has been driven by dramatic cost reductions and solar energy conversion efficiency enhancements. With new material systems and technologies emerging and old technologies maturing, it has been seen that solar cell performance optimization can be divided into three parts: 1) materials, 2) devices, and 3) photonics. Many emerging solar cell technologies, such as organic and hybrid perovskite solar cells, still face major issues related to materials and device, limiting their performance and stability. But even in the well-studied silicon and III–V semiconductor platform, there are still material puzzles to solve, in particular regarding interface properties. Important and recent examples of the second class include silicon heterojunction (SHJ), silicon/III–V tandem, and other tandems of III–V and II–VI materials. While the announcements of new record efficiencies in those devices have been skyrocketing [1], a significantly larger amount of studies in which potentially promising material

Manuscript received May 23, 2019; revised July 5, 2019; accepted July 18, 2019. Date of publication August 5, 2019; date of current version October 28, 2019. This work was supported by tenure-track start-up funding from the University of Twente.

The author is with the Mesa+ Institute for Nanotechnology, University of Twente, Enschede 7522 NB, The Netherlands (e-mail: r.saive@utwente.nl).

Color versions of one or more of the figures in this paper are available online at <http://ieeexplore.ieee.org>.

Digital Object Identifier 10.1109/JPHOTOV.2019.2930409

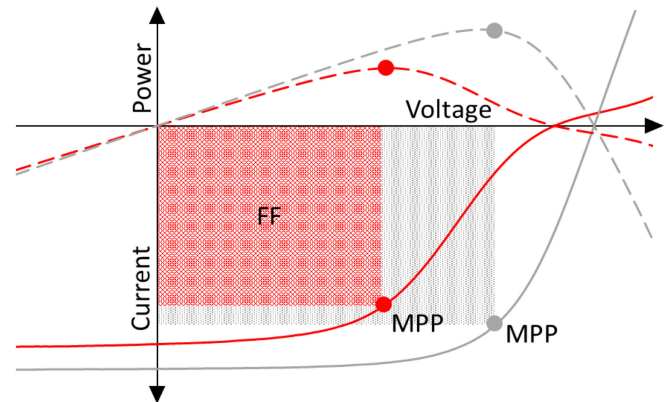


Fig. 1. Normal (gray curve) and s-shaped (red curve) I – V characteristics. The solid line shows the I – V curve, and the dashed line shows the power–voltage (P – V) curve.

combinations/device layouts failed to show success remain unheard of for the most part. One of the many problems that arise when performing research on new materials and their combinations is the appearance of s-shaped current–voltage (I – V) characteristics (e.g., [2]–[5]). In Fig. 1, an example of I – V curves is presented. The gray curve shows the standard behavior expected from an illuminated photodiode, and the red curve shows an example of an s-shaped I – V curve. In particular, in the CdSe community, the occurrence of s-shaped I – V curves is also referred to as roll-over (e.g., [6]).

The I – V characteristics of a solar cell determine its performance. Typically, the solar I – V curve follows a diode curve offset by the illumination-dependent short-circuit current I_L . In the ideal case, the current I depends on the voltage V as follows [7]:

$$I = I_0 \exp\left(\frac{qV}{k_B T}\right) - I_L. \quad (1)$$

To obtain a more realistic description of the I – V characteristics, one needs to also include the effect of series and shunt resistances. The former occurs, e.g., from high-resistivity absorber materials (vertical resistivity) or from lossy charge transport in the contact materials (lateral resistivity). Shunt resistances can occur through pin holes [8] or through the absence of properly performing minority charge carrier blocking layers [9]. With series resistance R_S and shunt resistance R_{SH} , the I – V dependence needs to be corrected to [7]

$$I = I_0 \exp\left(\frac{q(V + IR_S)}{k_B T}\right) + \frac{V + IR_S}{R_{SH}} - I_L. \quad (2)$$

The larger the R_S , the less steep the I - V curve at the position of the open-circuit voltage (V_{OC}) and the lower R_{SH} the less flat the curve at the position of the short-circuit current (e.g., [10]). Both high R_S and low R_{SH} decrease the fill factor (FF) of the solar cell. However, the simple modification with a constant series and a shunt resistance cannot explain the occurrence of s-shaped I - V curves [11]. Because of the s-shape, the FF becomes significantly reduced and often (but not necessarily) the mechanism that causes the s-shape also reduces V_{OC} and I_{sc} . The maximum power point moves significantly toward lower voltages for s-shaped I - V curves, as can be seen in Fig. 1.

This paper provides a review of the occurrence of s-shaped I - V curves in different material systems with the aim to facilitate their mitigation in ongoing and future solar cell research. Successful mitigation strategies as well as studies on the root cause of s-shaped curves will be presented for silicon, organic, perovskite, and inorganic thin-film solar cells. The observations for all material systems are unified to provide general guidelines on how to resolve the issue of s-shaped I - V characteristics.

II. S-SHAPED I - V CURVES IN SILICON HETEROJUNCTION SOLAR CELLS

The first silicon p-n junction solar cell was demonstrated in 1954 [12] and, hence, the silicon platform constitutes the most mature solar cell technology. Nevertheless, the record efficiency increase in monocrystalline silicon solar cells plateaued in the 1990s [13] at a value of approximately 24% [14], [15], still far away from the thermodynamic efficiency limit of 32% [16], [17] as well as from the practical, Auger recombination limited theoretical efficiency maximum of 29.4% [18]. At the same time, a new silicon architecture was invented: SHJ solar cells [19]. Taking advantage of the excellent passivation properties of amorphous silicon (a-Si), it became possible to reduce the surface recombination velocity and thereby enable V_{OC} of more than 750 mV [20]. Furthermore, p- and n-doped a-Si provides selective hole and electron contacts, which facilitates the charge carrier extraction [21]. This principle is shown in a simplified band diagram in Fig. 2. The black curve shows the band structure of silicon with ideal selective hole and electron contact. In 2014, the SHJ technology surpassed other monocrystalline technologies for the first time [13], [22], [23], and a combination of a-Si passivation together with interdigitated back contacts (IBC) [1] is currently holding the world record efficiency [1], [24]. Despite this success with a-Si passivation, there is still room for improvement in I_{sc} , V_{OC} , and FF as can be seen by the comparison between the current record [1], [24] and the Auger limit [18]. A major loss mechanism when using a-Si is the parasitic absorption within a-Si [25], [26] and within the transparent conductive oxides (TCOs) [25], [27] that are needed to assist the lateral charge transport. Great effort has been devoted to replace a-Si [28]–[36] and the TCOs [37]–[39] by less absorbing and more conductive materials [26], [40]. A more detailed overview of the history and device physics of SHJ solar cells has recently been published by Chavali *et al.* [11]. S-shaped I - V curves have commonly occurred in SHJ solar cells with a-Si [4], [11], [41]–[43] as well as with alternative emitter

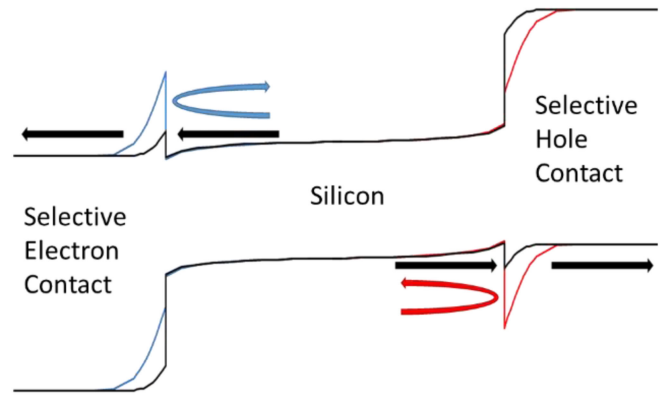


Fig. 2. Schematic of SHJ with selective hole and electron contact. The black curve shows the ideal case with low loss charge carrier extraction. The blue band alignment creates a barrier for electron extraction, and the red band alignment creates a barrier for hole extraction. (Band structures obtained from AFORS-HET simulation.)

materials [30], [44]. Examples will be presented in the following section.

A. Silicon Heterojunction Solar Cells With Amorphous Silicon Passivating Contacts

In this section, the occurrence of s-shaped I - V curves is discussed in standard SHJ solar cells, i.e., in SHJ solar cells in which passivation and selective charge extraction is achieved using a-Si. Lu *et al.* observed that while intrinsic a-Si as a passivation layer increases the V_{OC} and I_{sc} because of reduced surface recombination in IBC-SHJ solar cells, an s-shape and, therefore, lower FF are introduced [4]. The s-shape becomes more pronounced with thicker intrinsic a-Si layer, which the authors explain and model with a mismatch in valence band alignment [4]. They conclude that a thin, low-bandgap, high-quality, and high-conductivity layer of intrinsic a-Si should provide the optimum between good passivation for high V_{OC} and I_{sc} and good transport properties for high FF. Similarly, Allen *et al.* concluded that s-shaped curves are mainly influenced by the intrinsic a-Si bandgap and by defect states in the p-doped a-Si [45]. A correlation between s-shaped I - V curves and the presence of a transport barrier caused by a large valence band offset between crystalline and a-Si was also modeled by Chavali *et al.* [11], [43]. In a different study, Chavali *et al.* also found that s-shapes become less pronounced with increasing temperature [46], which also confirms the charge transport barrier theory [46]. Centurioni and Iencinella also observed that the TCO contact layer can have an influence on the shape of the I - V characteristics [47].

B. Silicon Heterojunction Solar Cells With Alternative Passivating Contacts

Battaglia *et al.* observed s-shaped I - V curves when replacing a-Si with MoOx [30]. They indicate unfavorable band alignment at the Si/MoOx interface as the culprit and obtained improved results with thinner layers (10 nm) of MoOx [30]. Geissbuehler *et al.* observed that s-shaped I - V curves appeared in Si/MoOx

SHJ solar cells only when annealing beyond 130 °C and, therefore, concluded that the annealing temperature needs to be kept low in order to avoid intermixing of layers that enhance charge transport blocking [36]. Annealing was also found to harm the FF of SHJ solar cells with metal oxide selective contacts in a study performed by Bivour *et al.* [48]. In a study on GaP as selective contact material, s-shaped behavior was observed, which vanished after highly doping the crystalline silicon at the interface [44]. Via X-ray photoelectron spectroscopy and cross-sectional scanning Kelvin probe microscopy, a high conduction band offset and subsequently a high charge transport barrier was identified as the culprit [44]. Seif *et al.* replaced the intrinsic a-Si by intrinsic a-SiO_x and found a thickness-dependent FF similar to the observation with intrinsic a-Si made by Lu *et al.* [4] and Shu *et al.* [41].

Nogay *et al.* experimentally studied the temperature dependence of I - V curves and found an onset of s-shaped behavior below room temperature that they were able to shift to lower temperatures when replacing p-doped a-Si by p-doped nanocrystalline silicon [49].

In conclusion, the observation of s-shaped I - V curves in SHJ solar cells has been linked to barriers in charge transport. These barriers were either created through a mismatch in band alignment with the selective contact [30], [36], [44] or with the passivation layer [4], [35], [41]. Fig. 2 shows a schematic of the band structure of silicon with a selective hole and a selective electron contact, without an intrinsic buffer/passivation layer. This band structure was created through AFORS-HET [50] modelling. The ideal alignment is shown as black curve; charge carrier extraction occurs without loss. The blue curve shows a barrier for electron extraction, and the red curve shows a barrier for hole extraction. Injection-level-dependent open-circuit voltage measurements (Suns- V_{oc}) [51] have shown to be a successful method to determine the height of these barriers [48], [52], [53]. Glunz *et al.* showed that Suns- V_{oc} can be used to determine the rear contact Schottky barrier height in silicon homojunction solar cells [53]. In SHJ solar cells, Bivour *et al.* found that the barrier height measured with Suns- V_{oc} indeed correlates with the s-shape strength of their solar cells and was decreased upon increasing the p-doping of the a-Si because of a more favorable band alignment [52] similar to the scenario shown in Fig. 2. In such a scenario, higher interface doping or higher temperature facilitates overcoming of barriers. Therefore, the model of interface band mismatch is consistent with the observation of decreased s-shape strength upon interface doping or heating.

To describe such charge transport energy barriers in an equivalent electrical circuit, it has been proposed to add a diode in series that acts in reverse to the main junction diode. In the case of the contact layer being a metal (but this is also applicable to degenerate semiconductors), a Schottky diode with a shunt resistor was proposed by Glunz *et al.* [53]. In the thermionic emission model, the dark/reverse current of a Schottky diode is proportional to $\exp(-q\Phi_B/k_B T)$, with Φ_B being the barrier height [54]. In addition to thermionic emission, tunneling through the junction also plays a role and is dependent on the width of the barrier (depletion zone) [55] which, in turn, is dependent on the doping

level [56]. The higher the doping, the narrower the depletion zone and, therefore, the higher the tunneling current. Although, these components can in principle be described in equivalent circuit models, the equations will only be valid for very specific scenarios and will have to be adjusted empirically for effects, such as (interface) recombination and doping-dependent barrier widths and heights. Therefore, more rigorous description of (s-shaped) I - V curves is offered by device solvers that take all bulk and interface effects of the semiconductor into account and solve the Poisson and continuity equations accordingly [57].

III. S-SHAPED I - V CHARACTERISTICS IN THIN-FILM SOLAR CELLS

The often referred to as second generation solar cells encompass material systems, such as CdTe, CuInSe₂ (CIS), CuInGaSe₂ (CIGS), and a-Si. These direct bandgap absorber materials enable complete light absorption within a few micrometers of film thickness, which allows for thin absorbers and, hence, thin solar cells. Furthermore, these cells can directly be fabricated on flexible metal foil substrates. The need of heterostructures is inherent in these systems to provide efficient charge carrier extraction. Thus, s-shaped I - V curves have been frequently observed in CdTe [6], [58], [59], copper indium (gallium) selenide [CI(G)S] [60]–[62], and a-Si cells [63]–[65].

A. CdTe Solar Cells

CdTe is the thin-film photovoltaics (PV) technology with the largest market share [66], and cell efficiencies of up to 21% have been demonstrated by First Solar [24]. For CdTe, the occurrence and dependence of s-shaped I - V curves have been thoroughly studied in experiments [6], [58] as well as in simulations [58]. In particular, in the CdTe community, the phenomenon s-shaped I - V curves is often referred to as “roll-over” [6], [67]–[73]. Similar to the SHJ solar cells, potential barriers with the contact materials have been proposed as the root cause. Interestingly, it was verified in numerical calculations [58], as well as in systematic experimental studies [6], that decreasing the barrier height directly translates into a less pronounced s-shape and a higher FF. Furthermore, it was investigated through simulations that an increase in the doping level of either the absorber or the contact material reduces the effect of the transport barrier and leads to higher FF [58]. In Fig. 3(a), the influence of contact doping on the I - V curve is shown, and in Fig. 3(b), this influence on the I - V curve is shown for the bulk doping [58]. It can be seen that in both cases, the FF increases with increasing doping. However, the effect and shape are slightly different for the different cases. If the bulk doping is increased, the curves are still s-shaped but with a higher FF, whereas with increasing contact doping, the situation can be changed from s-shaped to a normal I - V curve. This would point to the contact doping actually changing the band alignment, while the bulk doping only narrows the tunnel barrier. Such a model would also be consistent with the band alignment schematic presented in Fig. 2.

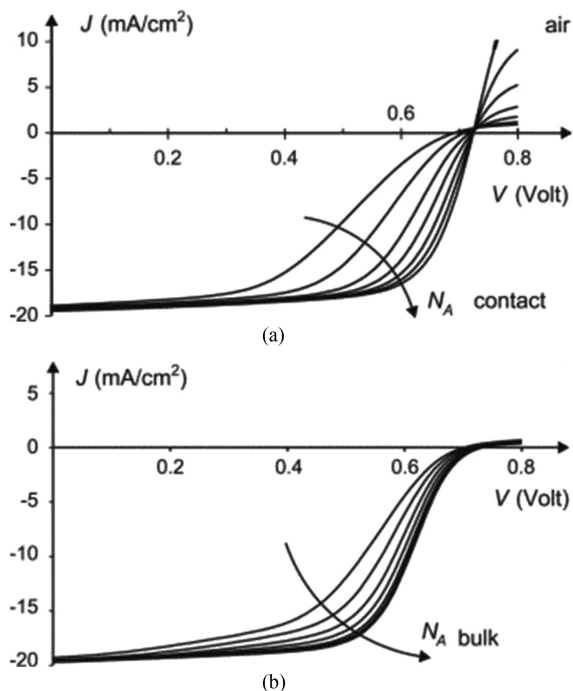


Fig. 3. Simulated I - V curves of CdTe solar cells with (a) increasing contact material doping and (b) increasing bulk doping. Recreated with permission from [58].

B. Copper Indium (Gallium) Selenide Solar Cells

First CI(G)S solar cells were introduced in the 1970s [74], [75], and the latest record energy conversion efficiency of 22.9% was demonstrated by Solar Frontier in 2017 [24]. S-shaped I - V curves have been frequently observed in experiments [59], [60], [76]–[80] and also been predicted in theoretical models [61], [77], [79], [81]. Similar to the other material systems, band discontinuities were found as the culprit in several experimental and theoretical studies. In addition, it was found that there can be a wavelength-dependent illumination dependence of the s-shaped I - V curve [59], [60], [78]. The authors explained this observation through trap states that can be filled and thereby made inactive depending on the illumination wavelength [60], [78]. This shows that although the s-shape itself is caused by an interface mismatch, the cause of the interface mismatch might lie in the presence of deep trap states in the contact layer. Numerical calculations were performed using the simulation software SCAPS [62], describing the influence of both trap states and band mismatch [61]. This should also be kept in mind when working with other materials systems and selective contacts that are prone to deep level trap states, such as molybdenum oxide [82].

C. Amorphous Silicon Solar Cells

First a-Si solar cells were introduced in the 1970s [83]. For a long time, their low cost and beneficial indoor performance ensured the highest share within the thin-film technology market [66]. a-Si was particularly popular for pocket calculators as these do not require high power [84]. Because of almost stagnating efficiency over the past 30 years, the market share of a-Si cells has been steadily decreasing [66]. Accordingly, solar

photovoltaics research has been focusing on the usage of a-Si not as the absorbing material, but rather as passivated contact materials, as described in detail above. However, studies that report s-shaped I - V curves in solar cells with a-Si absorber also found the barriers between absorber and charge transport layers to be the culprit [63]–[65], [85].

IV. S-SHAPED I - V CURVES IN ORGANIC SOLAR CELLS

All solar cells reported so far belong to the category of inorganic materials, which technically speaking means—apart from a few exceptions—the absence of carbon in the chemical compound. The discovery and development of conductive polymers in 1977 [86] gave momentum to the idea of organic semiconducting devices, which within the last decade found their way to the display, sensor, and solar market. Organic solar cell absorbers are either composed of small organic molecules, polymers, or a hybrid structure. Contact layers are often either organic [87] or inorganic materials [82] that provide the desired interface properties. Although, macroscopic device properties of organic solar cells resemble the ones of their inorganic cousins, there have been extensive debates on the origin of the photovoltage [88]–[91] and on charge carrier transport mechanisms [92]–[94]. S-shaped I - V curves have also been commonly observed in organic solar cells [3], [91], [95]–[106], and several studies have attempted to explain the occurrence within the framework of organic semiconductor charge transport [3], [91], [100], [102], [107].

One of the most thoroughly studied material systems in the organic photovoltaic community are poly(3-hexylthiophene):[6], [6]-phenyl-C61-butyric acid methyl ester (P3HT:PCBM) solar cells. S-shaped I - V curves have frequently been observed [2], [3], [95], [105]. Kumar *et al.* managed to tune the position of the I - V curve kink in P3HT:PCBM solar cells by introducing Bathocuprine (BCP) and V_2O_5 at the charge extraction interfaces [95]. Together with a theoretical model, they concluded that the s-shaped characteristics in their cells and similar devices [108] are caused by interface dipoles [95]. Ecker *et al.* also investigated P3HT:PCBM solar cells and found, with impedance spectroscopy, that a TiO_x selective charge transport layer causes s-shapes that disappear after UV soaking because of the decreased resistivity of the TiO_x [2]. Similar interface effects were also described as the cause for s-shaped I - V curves by Glatthaar *et al.* [109], and the importance of the electrodes was investigated by Jin *et al.* [110]. In a direct microscopic measurement, it was possible to visualize the described charge barrier in P3HT:PCBM solar cells [3]. In this measurement, a scanning electron microscopy/focused ion beam system was combined with a scanning probe system [111] to perform in-situ cross section preparation and measurement [112]. Fig. 4(a) shows the potential distribution across the cross section of three different solar cells with different s-shape strengths. The corresponding I - V curves are shown in Fig. 4(b). It can be seen that the potential drop at the P3HT:PCBM/Al interface increases with increasing s-shape signature in the I - V curve. In the same year, a similar electric field distribution was theoretically predicted by Tress and Inganäs [98]. They experimentally observed increased s-shape behavior strength with increased irradiance intensity.

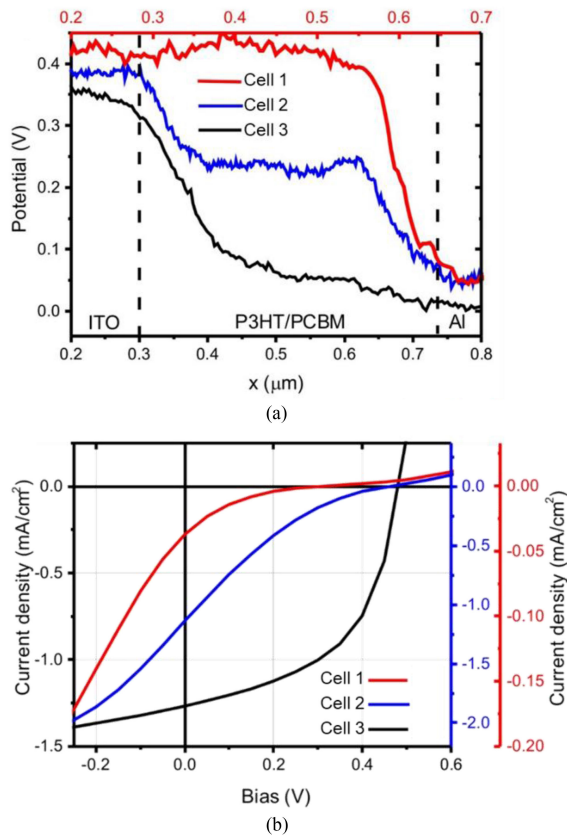


Fig. 4. (a) Measured potential distribution across the cross section of P3HT:PCBM solar cells. (b) Their corresponding I - V curves [91].

Further theoretical and experimental evidence was provided, and the importance of charge transport barriers at interfaces was also pointed out [104]. Finck and Schwartz, who performed drift-diffusion modeling of bulk heterojunction devices, observed that extraction of electrons near the cathode causes s-shapes [107]. This theory explained previous experimental results in which the s-shaped vanished upon the improvement of the cathode interface [101]. However, for flat/planar heterojunction solar cells, Tress *et al.* support the theory that s-shaped I - V curves can be caused by imbalanced mobilities [97], [99], [104]. In drift-diffusion models, they observed that a mismatch factor of more than 100 between hole mobility in the donor and the electron mobility in the acceptor material leads to the onset of s-shaped I - V curves in planar heterojunction organic solar cells [99]. A discussion of additional effects causing s-shaped I - V curves in organic solar cells can be found in [113].

S-shaped I - V curves were also observed in other organic and hybrid materials systems. Wagner *et al.* performed studies on the small molecule organic solar cell with donor-acceptor material combination of diindenoperylene and C_{60} . They observed that a good energetic alignment between the absorber and the contact materials, as well as purity of the absorber, is important in order to avoid s-shaped I - V curves. Wang *et al.* also investigated small molecule organic solar cells, which had copper phthalocyanine and C_{60} as an absorber material and observed that s-shapes were introduced and became more pronounced with increasing thickness of the exciton blocking layer BCP [100].

In poly(1,4-naphthalene vinylene) with CdTe nanocrystals, Chen *et al.* showed that the s-shape can be avoided using MoO_3 instead of PEDOT:PSS as a hole transport layer [103], which again shows the importance of appropriate selective contacts.

V. S-SHAPED I - V CURVES IN PEROVSKITE SOLAR CELLS

Perovskite solar cells have been fascinating the PV community because of their unprecedented rate of efficiency increase over the past 10 years [13]. Perovskite solar cells employ organic-inorganic hybrid compounds, such as methylammonium lead triiodide as the absorber layer [114] and received their name from the perovskite mineral (calcium titanate), which exhibits the same crystal structure [115]. From the first solar cell with an organic-inorganic halide absorber with an efficiency of 3.8% in 2009 [116], it took less than 10 years to reach an efficiency of 24.2% [13]. Despite this remarkable progress in efficiency, skepticism remains whether perovskite solar cells will be a viable means for power production because of inherent issues with materials instabilities [117]. In the early days of perovskite research, the occurrence of strong hysteresis when measuring I - V curves gave rise to debates [118]. The complex structure of the absorber materials, as well as the variety of modifications, naturally make perovskite solar cells very prone to also show s-shaped I - V curves. The list of reports in which s-shaped curves have been observed is long [119]–[128]:

Unger *et al.* observed enhanced s-shaped behavior after storing the cells in the dark and after light-soaking under reverse bias [120]. Werner *et al.* observed s-shapes that clearly changed strengths when changing the electrode sputtering parameters [121]. Using the method developed by Tress and Inganäs [98], they determined a hole extraction barrier as the culprit for the s-shapes [121]. Chemical degradation of the metal contact leading to charge extraction barriers was determined as the cause for the occurrence of s-shaped I - V curves by Guerrero *et al.* [122]. From drift-diffusion simulations, Koopmans and Koster derived that the only possible explanation for s-shaped curves in perovskite solar cells can be charge transport barriers at the absorber/contact interface [129]. Li *et al.* performed temperature-dependent I - V curve measurements and observed that by decreasing the temperature below room temperature s-shaped I - V curve appear [130]. This demonstrates a charge transport barrier that can be overcome through thermal excitation of the carriers [130] and was also seen in SHJ solar cells [46], as described above. Similar to the reports in CdTe presented above, Ge *et al.* showed that doping of the electron transport layer can mitigate s-shapes [131]. Overall, s-shaped I - V curves have been observed frequently in perovskite solar cells, and studies that aimed for an explanation of the occurrence determined charge transport barriers at the absorber/contact layer interface as the cause.

VI. CONCLUSION

The presented review shows that s-shaped I - V characteristics have been observed in a variety of solar cell materials systems. In almost all cases, a mismatch between the energy levels of the absorber layer and the charge extraction layers leading to a barrier for charge extraction was determined as the culprit for s-shaped I - V curves. Full mitigation of s-shapes was achieved

by adjusting the contacts, such as by using a different work function material [110] or by doping the contact layer [58]. Improvements of the FF without fully mitigating the s-shape was achieved by doping either absorber [44], [132] or selective contact materials [131]. Furthermore, decreasing the thickness of passivating [30], charge blocking [100], or buffer layers has been shown to mitigate s-shape I - V curves.

REFERENCES

- [1] K. Yoshikawa *et al.*, "Silicon heterojunction solar cell with interdigitated back contacts for a photoconversion efficiency over 26%," *Nature Energy*, vol. 2, 2017, Art. no. 17032.
- [2] B. Ecker, H.-J. Egelhaaf, R. Steim, J. R. Parisi, and E. von Hauff, "Understanding S-shaped current-voltage characteristics in organic solar cells containing a TiO_x interlayer with impedance spectroscopy and equivalent circuit analysis," *J. Phys. Chem. C*, vol. 116, no. 31, pp. 16333–16337, 2012.
- [3] R. Saive, C. Mueller, J. Schinke, R. Lovrincic, and W. Kowalsky, "Understanding S-shaped current-voltage characteristics of organic solar cells: Direct measurement of potential distributions by scanning Kelvin probe," *Appl. Phys. Lett.*, vol. 103, no. 24, 2013, Art. no. 243303.
- [4] M. Lu, U. Das, S. Bowden, S. Hegedus, and R. Birkmire, "Optimization of interdigitated back contact silicon heterojunction solar cells: Tailoring hetero-interface band structures while maintaining surface passivation," *Prog. Photovolt., Res. Appl.*, vol. 19, no. 3, pp. 326–338, 2011.
- [5] U. Das *et al.*, "Investigation of hetero-interface and junction properties in silicon heterojunction solar cells," in *Proc. 35th IEEE Photovolt. Spec. Conf.*, 2010, pp. 001358–001362.
- [6] X. Li *et al.*, "Roll-over behavior in current-voltage curve introduced by an energy barrier at the front contact in thin film CdTe solar cell," *Sol. Energy*, vol. 165, pp. 27–34, 2018.
- [7] P. Würfel and U. Würfel, *Physics of Solar Cells: From Basic Principles to Advanced Concepts*. Hoboken, NJ, USA: Wiley, 2016.
- [8] W. Qiu *et al.*, "Pinhole-free perovskite films for efficient solar modules," *Energy Environ. Sci.*, vol. 9, no. 2, pp. 484–489, 2016.
- [9] Y. Wu *et al.*, "Highly compact TiO_2 layer for efficient hole-blocking in perovskite solar cells," *Appl. Phys. Express*, vol. 7, no. 5, 2014, Art. no. 052301.
- [10] PV EDUCATION.ORG 2015. [Online]. Available: <http://pveducation.org/pvcdrom>
- [11] R. V. Chavali, S. De Wolf, and M. A. Alam, "Device physics underlying silicon heterojunction and passivating-contact solar cells: A topical review," *Prog. Photovolt., Res. Appl.*, vol. 26, no. 4, pp. 241–260, 2018.
- [12] D. M. Chapin, C. Fuller, and G. Pearson, "A new silicon p-n junction photocell for converting solar radiation into electrical power," *J. Appl. Phys.*, vol. 25, no. 5, pp. 676–677, 1954.
- [13] NREL. 2019. [Online]. Available: <https://www.nrel.gov/pv/cell-efficiency.html>
- [14] J. Zhao, A. Wang, P. P. Altermatt, S. R. Wenham, and M. A. Green, "24% efficient silicon solar cells," in *Proc. IEEE 1st World Conf. Photovolt. Energy Convers (Joint Conf. PVSC, PVSEC and PSEC)*, 1994, vol. 2, pp. 1477–1480.
- [15] M. A. Green and K. Emery, "Solar cell efficiency tables (version 4)," *Prog. Photovolt.*, vol. 2, pp. 231–234, 1994.
- [16] W. Shockley and H. J. Queisser, "Detailed balance limit of efficiency of p-n junction solar cells," *J. Appl. Phys.*, vol. 32, no. 3, pp. 510–519, 1961.
- [17] S. Rühle, "Tabulated values of the Shockley-Queisser limit for single junction solar cells," *Sol. Energy*, vol. 130, pp. 139–147, 2016.
- [18] A. Richter, M. Hermle, and S. W. Glunz, "Reassessment of the limiting efficiency for crystalline silicon solar cells," *IEEE J. Photovolt.*, vol. 3, no. 4, pp. 1184–1191, Oct. 2013.
- [19] M. Tanaka *et al.*, "Development of new a-Si/c-Si heterojunction solar cells: ACJ-HIT (artificially constructed junction-heterojunction with intrinsic thin-layer)," *Jpn. J. Appl. Phys.*, vol. 31, no. 11R, 1992, Art. no. 3518.
- [20] S. Y. Herasimenka, W. J. Dauksher, and S. G. Bowden, ">750 mV open circuit voltage measured on 50 μm thick silicon heterojunction solar cell," *Appl. Phys. Lett.*, vol. 103, no. 5, 2013, Art. no. 053511.
- [21] J. Haschke, O. Dupré, M. Boccard, and C. Ballif, "Silicon heterojunction solar cells: Recent technological development and practical aspects-from lab to industry," *Sol. Energy Mater. Sol. Cells*, vol. 187, pp. 140–153, 2018.
- [22] K. Masuko *et al.*, "Achievement of more than 25% conversion efficiency with crystalline silicon heterojunction solar cell," *IEEE J. Photovolt.*, vol. 4, no. 6, pp. 1433–1435, Nov. 2014.
- [23] M. A. Green, K. Emery, Y. Hishikawa, W. Warta, and E. D. Dunlop, "Solar cell efficiency tables (version 47)," *Prog. Photovolt., Res. Appl.*, vol. 24, pp. 3–11, 2016.
- [24] M. A. Green *et al.*, "Solar cell efficiency tables (version 53)," *Prog. Photovolt., Res. Appl.*, vol. 27, no. 1, pp. 3–12, 2019.
- [25] Z. C. Holman *et al.*, "Current losses at the front of silicon heterojunction solar cells," *IEEE J. Photovolt.*, vol. 2, no. 1, pp. 7–15, Jan. 2012.
- [26] R. Saive *et al.*, "Silicon heterojunction solar cells with effectively transparent front contacts," *Sustain. Energy Fuels*, vol. 1, pp. 593–598, 2017.
- [27] M. Morales-Masis, S. De Wolf, R. Woods-Robinson, J. W. Ager, and C. Ballif, "Transparent electrodes for efficient optoelectronics," *Adv. Electron. Mater.*, vol. 3, no. 5, 2017, Art. no. 1600529.
- [28] J. Bullock *et al.*, "Efficient silicon solar cells with dopant-free asymmetric heterocontacts," *Nature Energy*, vol. 1, 2016, Art. no. 15031.
- [29] J. Bullock, A. Cuevas, T. Allen, and C. Battaglia, "Molybdenum oxide MoO_x: A versatile hole contact for silicon solar cells," *Appl. Phys. Lett.*, vol. 105, no. 23, 2014, Art. no. 232109.
- [30] C. Battaglia *et al.*, "Silicon heterojunction solar cell with passivated hole selective MoO_x contact," *Appl. Phys. Lett.*, vol. 104, no. 11, 2014, p. Art. no. 113902.
- [31] W. Wu *et al.*, "Dopant-free multilayer back contact silicon solar cells employing V_2O_x /metal/ V_2O_x as an emitter," *RSC Adv.*, vol. 7, no. 38, pp. 23851–23858, 2017.
- [32] M. Bivour, J. Temmler, H. Steinkemper, and M. Hermle, "Molybdenum and tungsten oxide: High work function wide band gap contact materials for hole selective contacts of silicon solar cells," *Sol. Energy Mater. Sol. Cells*, vol. 142, pp. 34–41, 2015.
- [33] M. Feifel *et al.*, "Gallium phosphide window layer for silicon solar cells," *IEEE J. Photovolt.*, vol. 6, no. 1, pp. 384–390, Jan. 2016.
- [34] M. Feifel *et al.*, "MOVPE grown gallium phosphide-silicon heterojunction solar cells," *IEEE J. Photovolt.*, vol. 7, no. 2, pp. 502–507, Mar. 2017.
- [35] J. Peter Seif *et al.*, "Amorphous silicon oxide window layers for high-efficiency silicon heterojunction solar cells," *J. Appl. Phys.*, vol. 115, no. 2, 2014, Art. no. 024502.
- [36] J. Geissbühler *et al.*, "22.5% efficient silicon heterojunction solar cell with molybdenum oxide hole collector," *Appl. Phys. Lett.*, vol. 107, no. 8, 2015, Art. no. 081601.
- [37] L. Barraud *et al.*, "Hydrogen-doped indium oxide/indium tin oxide bilayers for high-efficiency silicon heterojunction solar cells," *Sol. Energy Mater. Sol. Cells*, vol. 115, pp. 151–156, 2013.
- [38] M. Morales-Masis, S. M. De Nicolas, J. Holovsky, S. De Wolf, and C. Ballif, "Low-temperature high-mobility amorphous IZO for silicon heterojunction solar cells," *IEEE J. Photovolt.*, vol. 5, no. 5, pp. 1340–1347, Sep. 2015.
- [39] E. Kobayashi, Y. Watabe, T. Yamamoto, and Y. Yamada, "Cerium oxide and hydrogen co-doped indium oxide films for high-efficiency silicon heterojunction solar cells," *Sol. Energy Mater. Sol. Cells*, vol. 149, pp. 75–80, 2016.
- [40] R. Saive and H. A. Atwater, "Mesoscale trumps nanoscale: Metallic mesoscale contact morphology for improved light trapping, optical absorption and grid conductance in silicon solar cells," *Opt. Express*, vol. 26, no. 6, pp. A275–A282, 2018.
- [41] Z. Shu, U. Das, J. Allen, R. Birkmire, and S. Hegedus, "Experimental and simulated analysis of front versus all-back-contact silicon heterojunction solar cells: Effect of interface and doped a-Si: H layer defects," *Prog. Photovolt., Res. Appl.*, vol. 23, no. 1, pp. 78–93, 2015.
- [42] E. Centurioni, D. Iencinella, R. Rizzoli, and F. Zignani, "Silicon heterojunction solar cell: A new buffer layer concept with low-temperature epitaxial silicon," *IEEE Trans. Electron Devices*, vol. 51, no. 11, pp. 1818–1824, Oct. 2004.
- [43] R. V. K. Chavali, J. R. Wilcox, B. Ray, J. L. Gray, and M. A. Alam, "Correlated nonideal effects of dark and light I - V characteristics in a-Si/c-Si heterojunction solar cells," *IEEE J. Photovolt.*, vol. 4, no. 3, pp. 763–771, May 2014.
- [44] R. Saive *et al.*, "Study of the interface in a GaP/Si heterojunction solar cell," *IEEE J. Photovolt.*, vol. 8, no. 6, pp. 1568–1576, Nov. 2018.
- [45] J. Allen, B. Shu, L. Zhang, U. Das, and S. Hegedus, "Interdigitated back contact silicon hetero-junction solar cells: The effect of doped layer defect levels and rear surface i-layer band gap on fill factor using two-dimensional simulations," in *Proc. 37th IEEE Photovolt. Spec. Conf.*, 2011, pp. 002545–002549.

- [46] R. V. K. Chavali *et al.*, "A generalized theory explains the anomalous suns- V_{oc} response of Si heterojunction solar cells," *IEEE J. Photovolt.*, vol. 7, no. 1, pp. 169–176, Jan. 2017.
- [47] E. Centurioni and D. Incinella, "Role of front contact work function on amorphous silicon/crystalline silicon heterojunction solar cell performance," *IEEE Electron Device Lett.*, vol. 24, no. 3, pp. 177–179, Mar. 2003.
- [48] M. Bivour, J. Temmler, F. Zähringer, S. Glunz, and M. Hermle, "High work function metal oxides for the hole contact of silicon solar cells," in *Proc. IEEE 43rd Photovolt. Spec. Conf.*, 2016, pp. 0215–0220.
- [49] G. Nogay *et al.*, "Nanocrystalline silicon carrier collectors for silicon heterojunction solar cells and impact on low-temperature device characteristics," *IEEE J. Photovolt.*, vol. 6, no. 6, pp. 1654–1662, Nov. 2016.
- [50] R. Varache *et al.*, "Investigation of selective junctions using a newly developed tunnel current model for solar cell applications," *Sol. Energy Mater. Sol. Cells*, vol. 141, pp. 14–23, 2015.
- [51] R. Sinton and A. Cuevas, "A quasi-steady-state open-circuit voltage method for solar cell characterization," in *Proc. 16th Eur. Photovolt. Sol. Energy Conf.*, 2000, vol. 1152.
- [52] M. Bivour *et al.*, "Doped layer optimization for silicon heterojunctions by injection-level-dependent open-circuit voltage measurements," *IEEE J. Photovolt.*, vol. 4, no. 2, pp. 566–574, Mar. 2014.
- [53] S. Glunz, J. Nekarda, H. Mäkel, and A. Cuevas, "Analyzing back contacts of silicon solar cells by Suns- V_{oc} -measurements at high illumination densities," *Presented at the 22nd Eur. Photovolt. Sol. Energy Conf. Exhib.*, 2007, vol. 3, p. 7.
- [54] D. K. Schroder, *Semiconductor Material and Device Characterization*. Hoboken, NJ, USA: Wiley, 2006.
- [55] J. Conley, C. Duke, G. Mahan, and J. Tiemann, "Electron tunneling in metal-semiconductor barriers," *Phys. Rev.*, vol. 150, no. 2, p. 466, 1966.
- [56] S. M. Sze and K. K. Ng, *Physics of Semiconductor Devices*. Hoboken, NJ, USA: Wiley, 2006.
- [57] M. Burgelman, P. Nollet, and S. Degraeve, "Modelling polycrystalline semiconductor solar cells," *Thin Solid Films*, vol. 361, pp. 527–532, 2000.
- [58] M. Burgelman, J. Verschraegen, S. Degraeve, and P. Nollet, "Analysis of CdTe solar cells in relation to materials issues," *Thin solid films*, vol. 480, pp. 392–398, 2005.
- [59] M. Köntges *et al.*, "Light induced changes in the electrical behavior of CdTe and Cu(In,Ga)Se₂ solar cells," *Thin Solid Films*, vol. 403, pp. 280–286, 2002.
- [60] I. Eisgruber, J. Granata, J. Sites, J. Hou, and J. Kessler, "Blue-photon modification of nonstandard diode barrier in CuInSe₂ solar cells," *Sol. Energy Mater. Sol. Cells*, vol. 53, no. 3/4, pp. 367–377, 1998.
- [61] M. Burgelman, J. Verschraegen, B. Minnaert, and J. Marlein, "Numerical simulation of thin film solar cells: Practical exercises with SCAPS," in *Proceedings of NUMOS [International Workshop on Numerical Modelling of Thin Film Solar Cells, Gent (B)]*. Gent, Belgium: UGent & Academia Press, 2007.
- [62] K. Decock, P. Zabierowski, and M. Burgelman, "Modeling metastabilities in chalcopyrite-based thin film solar cells," *J. Appl. Phys.*, vol. 111, no. 4, 2012, Art. no. 043703.
- [63] A. Dagamseh, B. Vet, F. Tichelaar, P. Sutta, and M. Zeman, "ZnO: Al films prepared by RF magnetron sputtering applied as back reflectors in thin-film silicon solar cells," *Thin Solid Films*, vol. 516, no. 21, pp. 7844–7850, 2008.
- [64] W. Kopetzky and R. Schwarz, "Numerical evaluation of amorphous silicon p-i-n solar cell degradation," *Appl. Phys. Lett.*, vol. 62, no. 23, pp. 2959–2961, 1993.
- [65] L. Veldhuizen *et al.*, "Optimization of hydrogenated amorphous silicon germanium thin films and solar cells deposited by hot wire chemical vapor deposition," *Thin Solid Films*, vol. 595, pp. 226–230, 2015.
- [66] Fraunhofer Institute for Solar Energy Systems, "Photovoltaics report," Fraunhofer Inst. Sol. Energy Syst., Freiburg, Germany, Mar. 2019. [Online]. Available: <https://www.ise.fraunhofer.de/content/dam/ise/de/documents/publications/studies/Photovoltaics-Report.pdf>
- [67] A. Niemegeers and M. Burgelman, "Effects of the Au/CdTe back contact on IV and CV characteristics of Au/CdTe/CdS/TCO solar cells," *J. Appl. Phys.*, vol. 81, no. 6, pp. 2881–2886, 1997.
- [68] N. Romeo, A. Bosio, R. Tedeschi, and V. Canevari, "Back contacts to CSS CdS/CdTe solar cells and stability of performances," *Thin Solid Films*, vol. 361, pp. 327–329, 2000.
- [69] G. Friesen, E. Dunlop, and R. Wendt, "Investigation of CdTe solar cells via capacitance and impedance measurements," *Thin Solid Films*, vol. 387, no. 1/2, pp. 239–242, 2001.
- [70] M. Gloeckler, A. Fahrenbruch, and J. Sites, "Numerical modeling of CIGS and CdTe solar cells: Setting the baseline," in *Proc. 3rd World Conf. Photovolt. Energy Convers.*, 2003, vol. 1, pp. 491–494.
- [71] C. Corwine, A. Pudov, M. Gloeckler, S. Demtsu, and J. Sites, "Copper inclusion and migration from the back contact in CdTe solar cells," *Sol. Energy Mater. Sol. Cells*, vol. 82, no. 4, pp. 481–489, 2004.
- [72] S. Demtsu and J. Sites, "Effect of back-contact barrier on thin-film CdTe solar cells," *Thin Solid Films*, vol. 510, no. 1/2, pp. 320–324, 2006.
- [73] X. Wu *et al.*, "Phase control of CuxTe film and its effects on CdS/CdTe solar cell," *Thin Solid Films*, vol. 515, no. 15, pp. 5798–5803, 2007.
- [74] L. Kazmerski, F. White, and G. Morgan, "Thin-film CuInSe₂/CdS heterojunction solar cells," *Appl. Phys. Lett.*, vol. 29, no. 4, pp. 268–270, 1976.
- [75] T. D. Lee and A. U. Ebong, "A review of thin film solar cell technologies and challenges," *Renewable Sustain. Energy Rev.*, vol. 70, pp. 1286–1297, 2017.
- [76] P. Schöppe *et al.*, "Rubidium segregation at random grain boundaries in Cu(In,Ga)Se₂ absorbers," *Nano Energy*, vol. 42, pp. 307–313, 2017.
- [77] F. W. Fecher, J. Adams, A. Vetter, C. Buerhop-Lutz, and C. J. Brabec, "Loss analysis on CIGS-modules by using contactless, imaging illuminated lock-in thermography and 2D electrical simulations," in *Proc. IEEE 40th Photovolt. Spec. Conf.* 2014, pp. 3331–3334.
- [78] W.-J. Lee *et al.*, "Behavior of photocarriers in the light-induced metastable state in the p-n heterojunction of a Cu(In,Ga)Se₂ solar cell with CBD-ZnS buffer layer," *ACS Appl. Mater. Interfaces*, vol. 8, no. 34, pp. 22151–22158, 2016.
- [79] M. Richter *et al.*, "Comprehensive simulation model for Cu(In,Ga)(Se,S)₂ solar cells," *Sol. Energy Mater. Sol. Cells*, vol. 132, pp. 162–171, 2015.
- [80] N. Naghavi *et al.*, "Chemical deposition methods for Cd-free buffer layers in CI(G)S solar cells: Role of window layers," *Thin Solid Films*, vol. 519, no. 21, pp. 7600–7605, 2011.
- [81] X. Sun *et al.*, "A physics-based compact model for CIGS and CdTe solar cells: From voltage-dependent carrier collection to light-enhanced reverse breakdown," in *Proc. IEEE 42nd Photovolt. Spec. Conf.*, 2015, pp. 1–6.
- [82] J. Meyer *et al.*, "Transition metal oxides for organic electronics: Energetics, device physics, and applications," *Adv. Mater.*, vol. 24, no. 40, pp. 5408–5427, 2012.
- [83] D. E. Carlson and C. R. Wronski, "Amorphous silicon solar cell," *Appl. Phys. Lett.*, vol. 28, no. 11, pp. 671–673, 1976.
- [84] H. Kodaira, Small-sized electronic calculator, Google Patents US4264962A, 1981.
- [85] B. Rech *et al.*, "Texture etched ZnO: Al films as front contact and back reflector in amorphous silicon pin and n-i-p solar cells," in *Conf. Rec. 26th IEEE Photovolt. Spec. Conf.*, 1997, pp. 619–622.
- [86] C. K. Chiang *et al.*, "Electrical conductivity in doped polyacetylene," *Phys. Rev. Lett.*, vol. 39, no. 17, pp. 1098–1101, 1977.
- [87] X. Crispin *et al.*, "The origin of the high conductivity of poly (3, 4-ethylenedioxythiophene)- poly (styrenesulfonate)(PEDOT- PSS) plastic electrodes," *Chem. Mater.*, vol. 18, no. 18, pp. 4354–4360, 2006.
- [88] L. Dou *et al.*, "25th anniversary article: A decade of organic/polymeric photovoltaic research," *Adv. Mater.*, vol. 25, no. 46, pp. 6642–6671, 2013.
- [89] C. J. Brabec *et al.*, "Origin of the open circuit voltage of plastic solar cells," *Adv. Funct. Mater.*, vol. 11, no. 5, pp. 374–380, 2001.
- [90] R. Saive *et al.*, "Imaging the electric potential within organic solar cells," *Adv. Funct. Mater.*, vol. 23, no. 47, pp. 5854–5860, 2013.
- [91] R. Saive, "Investigation of the potential distribution within organic solar cells by scanning Kelvin probe microscopy," Ph.D. dissertation, Univ. Heidelberg, Heidelberg, Germany, 2014.
- [92] H. Bässler, "Charge transport in disordered organic photoconductors a Monte Carlo simulation study," *Phys. Status Solidi (b)*, vol. 175, no. 1, pp. 15–56, 1993.
- [93] J.-L. Brédas, J. P. Calbert, D. da Silva Filho, and J. Cornil, "Organic semiconductors: A theoretical characterization of the basic parameters governing charge transport," *Proc. Nat. Acad. Sci. USA*, vol. 99, no. 9, pp. 5804–5809, 2002.
- [94] A. Kahn, N. Koch, and W. Gao, "Electronic structure and electrical properties of interfaces between metals and π -conjugated molecular films," *J. Polym. Sci. B, Polym. Phys.*, vol. 41, no. 21, pp. 2529–2548, 2003.
- [95] A. Kumar, S. Sista, and Y. Yang, "Dipole induced anomalous S-shape I-V curves in polymer solar cells," *J. Appl. Phys.*, vol. 105, no. 9, 2009, Art. no. 094512.

- [96] C. Uhrich *et al.*, "Organic thin-film photovoltaic cells based on oligothiophenes with reduced bandgap," *Adv. Funct. Mater.*, vol. 17, no. 15, pp. 2991–2999, 2007.
- [97] W. Tress, S. Corvers, K. Leo, and M. Riede, "Investigation of driving forces for charge extraction in organic solar cells: Transient photocurrent measurements on solar cells showing s-shaped current–voltage characteristics," *Adv. Energy Mater.*, vol. 3, no. 7, pp. 873–880, 2013.
- [98] W. Tress and O. Inganäs, "Simple experimental test to distinguish extraction and injection barriers at the electrodes of (organic) solar cells with S-shaped current–voltage characteristics," *Sol. Energy Mater. Sol. Cells*, vol. 117, pp. 599–603, 2013.
- [99] W. Tress *et al.*, "Imbalanced mobilities causing S-shaped IV curves in planar heterojunction organic solar cells," *Appl. Phys. Lett.*, vol. 98, no. 6, p. 23, 2011.
- [100] J. Wang, X. Ren, S. Shi, C. Leung, and P. K. Chan, "Charge accumulation induced S-shape J–V curves in bilayer heterojunction organic solar cells," *Org. Electron.*, vol. 12, no. 6, pp. 880–885, 2011.
- [101] B. Tremolet de Villers, C. J. Tassone, S. H. Tolbert, and B. J. Schwartz, "Improving the reproducibility of P3HT:PCBM solar cells by controlling the PCBM/cathode interface," *J. Phys. Chem. C*, vol. 113, no. 44, pp. 18978–18982, 2009.
- [102] J. Wagner *et al.*, "Identification of different origins for s-shaped current voltage characteristics in planar heterojunction organic solar cells," *J. Appl. Phys.*, vol. 111, no. 5, 2012, Art. no. 054509.
- [103] Z. Chen *et al.*, "Inverted hybrid solar cells from aqueous materials with a PCE of 3.61%," *Adv. Energy Mater.*, vol. 3, no. 4, pp. 433–437, 2013.
- [104] W. Tress, K. Leo, and M. Riede, "Influence of hole-transport layers and donor materials on open-circuit voltage and shape of I–V curves of organic solar cells," *Adv. Funct. Mater.*, vol. 21, no. 11, pp. 2140–2149, 2011.
- [105] A. Wagenpahl, D. Rauh, M. Binder, C. Deibel, and V. Dyakonov, "S-shaped current-voltage characteristics of organic solar devices," *Phys. Rev. B*, vol. 82, no. 11, 2010, Art. no. 115306.
- [106] M. R. Lilliedal, A. J. Medford, M. V. Madsen, K. Norrman, and F. C. Krebs, "The effect of post-processing treatments on inflection points in current–voltage curves of roll-to-roll processed polymer photovoltaics," *Sol. Energy Mater. Sol. Cells*, vol. 94, no. 12, pp. 2018–2031, 2010.
- [107] B. Y. Finck and B. J. Schwartz, "Understanding the origin of the S-curve in conjugated polymer/fullerene photovoltaics from drift-diffusion simulations," *Appl. Phys. Lett.*, vol. 103, no. 5, 2013, Art. no. 053306.
- [108] A. Geiser *et al.*, "Poly (3-hexylthiophene)/C60 heterojunction solar cells: Implication of morphology on performance and ambipolar charge collection," *Sol. Energy Mater. Sol. Cells*, vol. 92, no. 4, pp. 464–473, 2008.
- [109] M. Glatthaar *et al.*, "Efficiency limiting factors of organic bulk heterojunction solar cells identified by electrical impedance spectroscopy," *Sol. Energy Mater. Sol. Cells*, vol. 91, no. 5, pp. 390–393, 2007.
- [110] H. Jin *et al.*, "Polymer–electrode interfacial effect on photovoltaic performances in poly (3-hexylthiophene): Phenyl-C₆₁-butyric acid methyl ester based solar cells," *J. Phys. Chem. C*, vol. 113, no. 38, pp. 16807–16810, 2009.
- [111] R. Saive, L. Mueller, E. Mankel, W. Kowalsky, and M. Kroeger, "Doping of TIPS-pentacene via focused ion beam (FIB) exposure," *Org. Electron.*, vol. 14, no. 6, pp. 1570–1576, 2013.
- [112] M. Scherer, R. Saive, D. Daume, M. Kröger, and W. Kowalsky, "Sample preparation for scanning Kelvin probe microscopy studies on cross sections of organic solar cells," *AIP Adv.*, vol. 3, no. 9, 2013, Art. no. 092134.
- [113] W. Tress, "Organic solar cells," in *Organic Solar Cells*. New York, NY, USA: Springer, 2014, pp. 67–214.
- [114] W.-J. Yin, J.-H. Yang, J. Kang, Y. Yan, and S.-H. Wei, "Halide perovskite materials for solar cells: A theoretical review," *J. Mater. Chem. A*, vol. 3, no. 17, pp. 8926–8942, 2015.
- [115] P. Gao, M. Grätzel, and M. K. Nazeeruddin, "Organohalide lead perovskites for photovoltaic applications," *Energy Environ. Sci.*, vol. 7, no. 8, pp. 2448–2463, 2014.
- [116] A. Kojima, K. Teshima, Y. Shirai, and T. Miyasaka, "Organometal halide perovskites as visible-light sensitizers for photovoltaic cells," *J. Amer. Chem. Soc.*, vol. 131, no. 17, pp. 6050–6051, 2009.
- [117] M. Saliba *et al.*, "Cesium-containing triple cation perovskite solar cells: Improved stability, reproducibility, and high efficiency," *Energy Environ. Sci.*, vol. 9, no. 6, pp. 1989–1997, 2016.
- [118] H. J. Snaith *et al.*, "Anomalous hysteresis in perovskite solar cells," *J. Phys. Chem. Lett.*, vol. 5, no. 9, pp. 1511–1515, 2014.
- [119] W. Tress *et al.*, "Understanding the rate-dependent J–V hysteresis, slow time component, and aging in CH₃NH₃PbI₃ perovskite solar cells: The role of a compensated electric field," *Energy Environ. Sci.*, vol. 8, no. 3, pp. 995–1004, 2015.
- [120] E. L. Unger *et al.*, "Hysteresis and transient behavior in current–voltage measurements of hybrid-perovskite absorber solar cells," *Energy Environ. Sci.*, vol. 7, no. 11, pp. 3690–3698, 2014.
- [121] J. Werner *et al.*, "Sputtered rear electrode with broadband transparency for perovskite solar cells," *Sol. Energy Mater. Sol. Cells*, vol. 141, pp. 407–413, 2015.
- [122] A. Guerrero *et al.*, "Interfacial degradation of planar lead halide perovskite solar cells," *ACS Nano*, vol. 10, no. 1, pp. 218–224, 2015.
- [123] M. Alifanti, M. Florea, S. Somacescu, and V. Parvulescu, "Supported perovskites for total oxidation of toluene," *Appl. Catal. B, Environ.*, vol. 60, no. 1–2, pp. 33–39, 2005.
- [124] C. Bi, B. Chen, H. Wei, S. DeLuca, and J. Huang, "Efficient flexible solar cell based on composition-tailored hybrid perovskite," *Adv. Mater.*, vol. 29, no. 30, 2017, Art. no. 1605900.
- [125] M. Lee, Y. Ko, and Y. Jun, "Efficient fiber-shaped perovskite photovoltaics using silver nanowires as top electrode," *J. Mater. Chem. A*, vol. 3, no. 38, pp. 19310–19313, 2015.
- [126] Y. Cheng *et al.*, "Spectroscopic study on the impact of methylammonium iodide loading time on the electronic properties in perovskite thin films," *J. Mater. Chem. A*, vol. 4, no. 2, pp. 561–567, 2016.
- [127] F. Jiang *et al.*, "A two-terminal perovskite/perovskite tandem solar cell," *J. Mater. Chem. A*, vol. 4, no. 4, pp. 1208–1213, 2016.
- [128] Z. Lin *et al.*, "Interface studies of the planar heterojunction perovskite solar cells," *Sol. Energy Mater. Sol. Cells*, vol. 157, pp. 783–790, 2016.
- [129] M. K. Koopmans and J. A., "A numerical study of the implications of s-shaped JV characteristics in perovskite solar cells," presented at the Physics at Veldoven, Jan. 2019.
- [130] C. Li *et al.*, "Thermionic emission-based interconnecting layer featuring solvent resistance for monolithic tandem solar cells with solution-processed perovskites," *Adv. Energy Mater.*, vol. 8, no. 36, 2018, Art. no. 1801954.
- [131] R. Ge, F. Qin, L. Hu, S. Xiong, and Y. Zhou, "High fill factor over 82% enabled by a biguanide doping electron transporting layer in planar perovskite solar cells," *Front. Optoelectron.*, vol. 11, no. 4, pp. 360–366, 2018.
- [132] L. Hu *et al.*, "An amidine-type n-dopant for solution-processed field-effect transistors and perovskite solar cells," *Adv. Funct. Mater.*, vol. 27, no. 41, 2017, Art. no. 1703254.